Degradation of sulfamethoxazole by heat-activated persulfate oxidation: elucidation of the degradation mechanism and influence of process parameters

Hannah Milh, Ben Schoenaers, Andre Stesmans, Deirdre Cabooter, Raf Dewil

PII: S1385-8947(19)31628-6
DOI: https://doi.org/10.1016/j.cej.2019.122234
Article Number: 122234
Reference: CEJ 122234

To appear in: *Chemical Engineering Journal*

Received Date: 26 April 2019
Revised Date: 10 July 2019
Accepted Date: 13 July 2019

Please cite this article as: H. Milh, B. Schoenaers, A. Stesmans, D. Cabooter, R. Dewil, Degradation of sulfamethoxazole by heat-activated persulfate oxidation: elucidation of the degradation mechanism and influence of process parameters, *Chemical Engineering Journal* (2019), doi: https://doi.org/10.1016/j.cej.2019.122234

Degradation of sulfamethoxazole by heat-activated persulfate oxidation: elucidation of the degradation mechanism and influence of process parameters

Hannah Milh [a], Ben Schoenaers [b], Andre Stesmans [b], Deirdre Cabooter [c], Raf Dewil [a,*]

[a] *KU Leuven, Department of Chemical Engineering, Process and Environmental Technology Lab, J. De Nayerlaan 5, 2860 Sint-Katelijne-Waver, Belgium*

[b] *KU Leuven, Department of Physics and Astronomy, Lab for Semiconductor Physics, Celestijnenlaan 200d, 3001 Leuven, Belgium*

[c] *KU Leuven, Department of Pharmaceutical and Pharmacological Sciences, Lab of Pharmaceutical Analysis, Herestraat 49, 3000 Leuven, Belgium*

e-mail: raf.dewil@kuleuven.be (R. Dewil)

Highlights

- Investigation of process conditions for the degradation of sulfamethoxazole
- Identification of degradation products for elucidation of the degradation mechanism
- Elucidation of pH influence on formation of degradation products

Abstract

In this article, heat-activated persulfate oxidation was investigated as a promising technique for the removal of sulfamethoxazole from an aqueous environment. It was found that the degradation efficiency of sulfamethoxazole increases with increasing persulfate concentration due to the increased $\bullet SO_4^-$ production. As suggested by the Arrhenius equation, the sulfamethoxazole degradation rate constant increased with increasing temperature. An activation energy of 103 kJ/mol was determined. Furthermore, the initial pH of the reaction mixture had a large influence on the degradation of sulfamethoxazole. At higher initial pH values, the degradation of sulfamethoxazole increased. The main cause for this increase is a difference in sulfamethoxazole distribution: at higher pH, the deprotonated form of sulfamethoxazole is present and found to be more susceptible to degradation. A second reason was found to be the formation of •OH at higher initial pH values, although this contribution was smaller. To elucidate the degradation process, six intermediates were identified, and the difference in formation of these compounds at different initial pH values was revealed. Through ECOSAR modeling, some degradation products were found to be of main interest when monitoring the toxicity of the degradation mixture.

Keywords

Sulfamethoxazole, heat-activated persulfate oxidation, SR-AOP, degradation mechanism, toxicity evaluation

1. Introduction

The presence of pharmaceuticals in wastewater has become a topic of increasing concern, which is mainly caused by the growing production (and consumption) of pharmaceuticals due to (*i*) the growing world population, (*ii*) the ageing of this population and (*iii*) an increasing food production (use of antibiotics for the enhancement of livestock production) [1]. Both diffuse sources, i.e., the presence of pharmaceuticals in municipal wastewater because of the excretion of non-metabolized pharmaceuticals, and point sources mainly consisting of pharmaceutical industry effluent contribute to the problem [2]. Traces of pharmaceutical compounds in aquatic systems are of major concern due to their possible ecological impact on aquatic organisms (e.g., endocrine disruption and increase of antibiotic resistant bacteria due to the presence of antibacterial drugs) [3]. Moreover, many of these pharmaceuticals possess unknown chronic effects [4]. The concentration of most pharmaceuticals in aqueous environments is usually quite low, and it is only due to the developments in chromatographic techniques and mass spectrometry (MS) that their quantification in various environmentally relevant media has become possible. Therefore, the problem of their presence in the environment has only emerged recently, and the establishment of appropriate legal frameworks are often still in progress [4].

Conventional wastewater treatment plants are often inadequate to remove pharmaceutical products from wastewater due to their non-biodegradable nature [1]. Recent developments in techniques for removal of pharmaceuticals from aquatic environments include adsorption, ozonation, membrane techniques, AOPs (Advanced Oxidation Processes) and many others [1,4]. AOPs are widely known processes that make use of the generation of the highly reactive OH radical (•OH) to oxidize target pollutants. Recently, increasing interest has been shown in sulfate radical based AOPs (SR-AOP), in which the sulfate radical ($\bullet SO_4^-$) (partially) takes over the role of oxidant [5]. The use of $\bullet SO_4^-$ has many advantages over •OH. First, $\bullet SO_4^-$ has an equal or higher oxidation potential (2.5 – 3 V, at acidic-neutral pH) than •OH (2.7 V). Secondly,

•SO_4^- has a higher selectivity: whereas •OH can react with the target pollutants in three different ways (electron transfer, hydrogen abstraction and addition reaction), •SO_4^- mainly react via electron transfer, making it a much more selective oxidant. •SO_4^- also has a longer half-life than •OH (30-40 µs compared to <1 µs respectively). Using •SO_4^- instead of •OH was also found to result in a higher mineralization rate [6]. Sulfate radicals are most often generated via the activation of the precursors persulfate (PS, $S_2O_8^{2-}$) or peroxymonosulfate (PMS, HSO_5^-). Two of the most frequently used activation methods are (*i*) the use of transition metals (heterogeneous/homogenous) and (*ii*) UV or heat activation.

The activation of PS and PMS using transition metals is based on a redox reaction between the transition metal and the precursor (Equations (1) and (2)). In these reactions, •SO_4^- radicals are formed. Different transition metals can be used, such as Fe^{2+} or Co^{2+} [7,8].

$$Me^{n+} + HSO_5^- \rightarrow Me^{n+1} + \cdot SO_4^- + OH^- \qquad (1)$$

$$Me^{n+} + S_2O_8^{2-} \rightarrow Me^{n+1} + \cdot SO_4^- + SO_4^{2-} \qquad (2)$$

UV radiation or thermal energy can be used to break the peroxide bond in the PS or PMS molecule to form radicals. In case of PS, in first instance, this results in the formation of •SO_4^- only, whereas in the case of PMS, both •SO_4^- and •OH are formed (Equations (3) and (4), respectively) [9]. Secondly, these formed radicals undergo transformation reactions resulting in the formation of other radicals (e.g., the transformation of •SO_4^- into •OH due to hydrolysis or reaction with OH^- ions) [6].

$$S_2O_8^{2-} \xrightarrow{\Delta/UV} 2 \cdot SO_4^- \qquad (3)$$

$$HSO_5^- \xrightarrow{\Delta/UV} \cdot SO_4^- + \cdot OH \qquad (4)$$

Next to these activation methods, others have been studied, including ultrasonic activation, alkaline activation, heterogeneous catalytic and electrochemical activation [10].

Recently, the use of heat-activated persulfate oxidation has gained specific interest [11,12]. The influence of various process variables on the degradation of a myriad of organic compounds has been described in some literature sources. For example, some authors [13,14] identified the PS concentration to be a major influential factor, which is positively correlated with the pollutant degradation efficiency. The pH dependence was studied and was attributed to a difference in relative abundancy of the radicals present in the reaction mixture [14,15]. Whereas the contribution of the different radicals has previously also been studied, only few authors have investigated the influence of pH hereon. Moreover, to the best of our knowledge, the influence of the pH on the produced radicals and the resulting degradation products has been studied even less. Ji et al. (2015) proposed a degradation pathway for sulfamethoxazole (SMX), including the presence of radicals other than $\bullet SO_4^-$ [16]. However, they focused on finding a general degradation pathway, whereas the aim in this paper is to obtain a detailed insight in how the degradation pathway is influenced by other radicals in a more quantitative way, and which degradation paths are favored when the radical distribution changes.

In this paper, the degradation of sulfamethoxazole (SMX), a widely used antibiotic, is investigated using heat-activated persulfate oxidation. The influence of different process variables, such as oxidant concentration, temperature and initial SMX concentration is examined. Furthermore, a more in-depth study of the influence of the initial pH value on the formation of different radicals and the contribution of these radicals to the degradation process is investigated. Subsequent to the elucidation of the degradation products formed in the process, the presence of the different radicals is correlated to the identified degradation products and their abundancy. To provide an estimate of the change in ecotoxicity of the SMX solution following the treatment, an ECOSAR screening of the formed degradation products is carried out as well.

2. Materials and methods

2.1 Chemicals

For the batch experiments, potassium persulfate ($K_2S_2O_8$, Fisher Scientific, Merelbeke, Belgium, reagent grade), ethanol (EtOH, Fisher Chemical, Merelbeke, Belgium, analytical reagent grade), potassium iodide (KI, Acros Organics, Geel, Belgium, 99+%), tert-butanol (TBA, Acros Organics, 99.5%), sodium bicarbonate ($NaHCO_3$, VWR, Leuven, Belgium, reagent grade), methanol (MeOH, Acros Organics, HPLC grade), sodium hydroxide (NaOH, Geel, Belgium, Acros Organics), sulfuric acid (H_2SO_4, Fisher Chemical, >95%) and sulfamethoxazole (SMX, TCI Europe, Zwijndrecht, Belgium, >98%) were used. Chemicals for High Pressure Liquid Chromatography (HPLC) analysis were acetonitrile (ACN, Fisher Chemical, HPLC grade) and formic acid (FA, Honeywell, Leuven, Belgium, ≥98%). LC-MS measurements were carried out using LC-MS grade acetonitrile (ACN, VWR) and FA (Acros Organics, 99%). For the quantification of intermediate m/z 99, the analytical standard 3-amino-5-methylisoxazole (TCI Europe, Belgium, >97%) was purchased. For the electron spin resonance (ESR) experiments dimethyl sulfoxide (DMSO, Acros Organics, 99.7%) and 5,5-dimethyl-1-pyrroline-N-oxide (DMPO, SanBio B.V., Uden, The Netherlands, ≥98%) were used. All solutions were made in ultrapure Milli Q water.

2.2 Experimental set-up

All experiments were carried out in a double walled, cylindrical borosilicate glass reactor. Heating of the reaction mixture was enabled by recirculating heated water through the reactor jacket. The reactor itself was placed on a stirring plate to ensure homogeneous mixing of the reaction mixture. In a typical experiment, the reactor was filled with 900 mL of a 100 ppm SMX solution (unless specified otherwise). The standard SMX concentration (100 ppm) was chosen to make sure the formed degradation products could be easily identified. When the solution was heated to its specified temperature, PS (in solid form) was added to initiate the reaction. For the experiments studying the influence of the pH, the pH was adjusted with NaOH or H_2SO_4. To

avoid possible scavenging reactions with the produced radicals, no additional buffer was used to control the pH. At defined time intervals, the temperature and pH inside the reactor were measured using a thermocouple (Hanna Instruments, HI 147-00) and a pH meter (Schott, CG 820), respectively, to follow up the reaction process. The different process variables tested were: (*i*) oxidant (PS) dose, (*ii*) temperature, (*iii*) initial SMX concentration and (*iv*) initial pH of the reaction mixture. To assess the degradation of SMX and consumption of PS for the different experiments, 5 mL samples were taken from the reactor at defined time intervals and analyzed as further specified. Each sample was introduced in a tube containing 5 mL MeOH to immediately quench any remaining sulfate radicals and stop the reaction. Thereafter, the sample was placed in an ice bath to further prevent activation of unreacted PS. All results shown with error bars were performed in triplicate unless stated otherwise.

2.3 Analytical techniques

The residual PS concentration was measured using a spectrophotometric method based on Liang et al. (2008) [17]. Depending on the initial PS concentration, a specific sample volume (500, 250 or 50 µL) was introduced in a tube. Then, 5 mL of a solution containing 5 g/L $NaHCO_3$ and 100 g/L KI were added, and the reaction mixture was homogenized. After 15 min, the absorbance of the reaction mixture was measured in a UV-VIS spectrophotometer (Shimadzu UV-1800) at a wavelength of 390 nm.

SMX concentrations were analyzed by HPLC-UV. For the HPLC-UV determination, an Agilent 1100 HPLC system (Agilent Technologies, Waldbronn, Germany) was used. The system consisted of a quaternary pump, an autosampler and a VWD detector. A C18 column (Zorbax Eclipse Plus, 4.6 x 100 mm; particle size (d_p): 3.5 µm) was used for the separation. The mobile phase was a mixture of (A) 0.1% FA in water and (B) ACN containing 0.1% FA. The elution method consisted of a gradient increasing from 10% to 95% B in 15 min, maintained at 95% B for 10 min, and then returned to the initial conditions for equilibration during 10 min.

The flow rate was set at 1 mL/min and the injection volume was 3 µL. SMX UV-detection was done at a wavelength of 280 nm.

For the identification experiments, an Agilent 1290 Infinity UHPLC system consisting of a 1290 quaternary pump, an autosampler and a diode array detector (DAD) (flow cell: 1 µL) was used. For the separation, two Acquity UPLC BEH C18 columns (2.1 x 100 mm; d_p 1.7 µm; Waters, Milford, USA) were coupled in series to increase the separation power [18]. The mobile phase consisted of (A) 0.1% FA in water and (B) ACN containing 0.1% FA. The applied gradient method consisted of an increase from 10% to 95% B in 16 min and a further increase to 100% in 0.5 min. 100% B was held for 1.5 min and subsequently returned to the initial conditions in 0.5 min (10% B). The initial conditions were held for 10 min to recondition the column. The flow rate was 0.2 mL/min and the injection volume 2 µL. The thermostat was kept at 30 °C. UV detection was carried out at a wavelength of 254 nm. The UHPLC system was coupled to a Bruker HCT Esquire 3000 plus ion trap mass spectrometer system, equipped with an ESI probe. The capillary voltage was set at +2 kV, with a drying gas flow rate of 7 L/min and a drying temperature of 365 °C. The nebulizer gas pressure was set at 30 psi. All samples were analyzed in positive ion mode. The scan range was set to 50-400 m/z in the first 15 min, and 130-400 m/z during the last 13.5 min of the analysis.

A multilevel calibration curve was constructed for SMX and m/z 99 at 8 concentration levels (0.03-50 mg/L) and 3 concentration levels (1-10 mg/l), respectively, in a matrix containing 5 mM PS. Each sample was injected 3 times. Over the entire range of concentrations, linear calibration curves with $R^2 > 0.99997$ and $R^2 > 0.99993$ and average RSDs below 3% were obtained for SMX and m/z 99, respectively (except at the LOQ where RSD ≤ 10%). The instrumental limits of detection (LOD) and quantification (LOQ) were determined by injecting solutions of decreasing concentrations. Considering a S/N ≥ 3 (n= 5) for the LOD and a S/N ≥

10 (RSD < 10%, n= 5) for the LOQ, the LOD and LOQ for SMX were 0.03 mg/L and 0.009 mg/L respectively. For m/z 99, the LOQ and LOD were 1 mg/L and 0.3 mg/L respectively.

2.4 ECOSAR screening

To assess the potential acute and chronic toxicity of the identified degradation products, the ECOSAR (ECOlogical Structure-Activity Relationship) predictive model, developed by the US Environmental Protection Agency was used as done in previous literature [19,20]. In terms of acute toxicity, 96-h Half Lethal Concentration (LC_{50}) for fish, 48-h LC_{50} for daphnia and 96-h Half Effective Concentration (EC_{50}) for green algae was estimated for every degradation product. For chronic toxicity, the Chronic Value (ChV) was determined.

2.5 Electron spin resonance (ESR) experiments

The ESR experiments were carried out using the method proposed by Zalibera et al. (2009) [21]. 5,5-dimethyl-1-pyrroline-N-oxide (DMPO) was used as spin trap. For every experiment, PS and pure DMPO were dissolved in dimethyl sulfoxide (DMSO) to obtain a concentration of 2 and 20 mM respectively. Then, heat activation of the solution was performed and an aliquot of the reaction mixture was placed in the ESR instrument using a Teflon sample holder. The ESR spectra were obtained at room temperature using a JEOL JES-FA100 (X-band, ~ 9.2 GHz) spectrometer. Conventional continuous wave absorption first derivative measurements were carried out with the use of periodic modulation $B_m cos(\omega_m t)$, at $\omega_m/2\pi \approx 100$ kHz of the applied magnetic field B. Spectrum g values were determined by making use of a co-mounted calibrated Mn^{2+} marker sample.

3. Results and discussion

3.1 Process kinetics

During all experiments, SMX degradation was measured over time to investigate the kinetics of the process. Pseudo first order kinetics for heat-activated persulfate oxidation were previously reported [16,22]. This assumption was verified and confirmed for all experiments by plotting $\ln([SMX]/[SMX]_0)$ as a function of time. If the degradation reaction indeed follows pseudo first order kinetics, a straight line is obtained with the observed reaction rate constant k_{obs} as its negative slope. As an example, Figure 1a shows the SMX degradation over time for one of the experiments. In Figure 1b, the fit for pseudo first order kinetics is shown. This results in an observed reaction rate constant of 0.0297 min^{-1} with an R^2 of 0.9929, hence confirming the validity of the pseudo first order kinetic model.

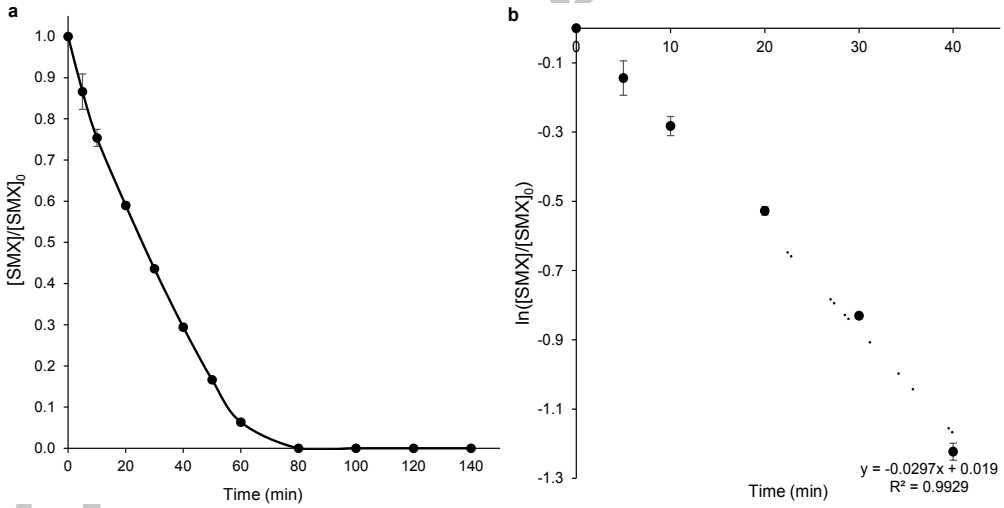

Figure 1: a) $[SMX]/[SMX]_0$ as a function of time; b) Determination of the process kinetics. Conditions: T= 70 °C, $[PS]_0$= 10 mM, $[SMX]_0$= 100 ppm.

3.2 Influence of oxidant concentration

The influence of the PS dose on the SMX degradation was assessed. Figure 2a shows the SMX degradation for different PS doses, ranging from 0 to 35 mM. The degradation rate increases with increasing initial PS dose $[PS]_0$. A spectrophotometric determination of PS after 140 min reaction time confirmed that a rest concentration of PS was present for every experiment in this section, indicating that PS was available for activation throughout the whole reaction and that

it was not stoichiometrically limiting the reaction. It was previously found that increasing PS concentration resulted in an increase of produced radicals, explaining the increase of SMX degradation rate at higher $[PS]_0$ [23].

The relationship between the PS dose and the reaction rate constant was determined in detail following the methodology previously suggested by Ma et al. (2017) [22]. The reaction rate *r* is defined as follows:

$$r = \frac{-d[SMX]}{dt} = k * [SMX]^a [PS]^b \quad (5)$$

In this equation, *r* is the reaction rate, *k* the reaction rate constant, and *a* and *b* the order of the reaction in SMX and PS, respectively. Factor *a* in Equation (5) will be equal to 1 if the reaction is of pseudo first order (which was confirmed earlier), and when using the definition for pseudo first order reaction kinetics, Equation (6) is valid, leading to the expression for k_{obs} as a function of *k* and [PS] (Equation (7)).

$$r = \frac{-d[SMX]}{dt} = k * [SMX]^a [PS]^b = k_{obs} * [SMX] \quad (6)$$

$$k_{obs} = k * [PS]^b \quad (7)$$

By taking the natural logarithm of Equation (7), this equation is transformed into Equation (8).

$$\ln(k_{obs}) = \ln(k) + b * ln([PS]) \quad (8)$$

When PS is present in large excess, [PS] will only vary limitedly throughout the reaction and thus can be equated to $[PS]_0$ to obtain Equation (9).

$$\ln(k_{obs}) = \ln(k) + b * \ln([PS]_0) \quad (9)$$

Equation (9) expresses the relationship between the SMX degradation (through k_{obs}) and the initial PS concentration. By plotting $\ln(k_{obs})$ against $\ln([PS]_0)$, a linear relationship is obtained, with the slope of the straight line that is produced equaling the reaction order of the

decomposition in PS (factor *b*). As depicted in Figure 2b, the linear fit of the obtained experimental results yields a slope (*b*) of 0.8699 with coefficient of determination R^2=0.9975. First order kinetics in PS was already suggested previously [24]. Therefore, factor *b* is expected to have a value close to 1. The obtained experimental value is hence in good agreement with previous observations.

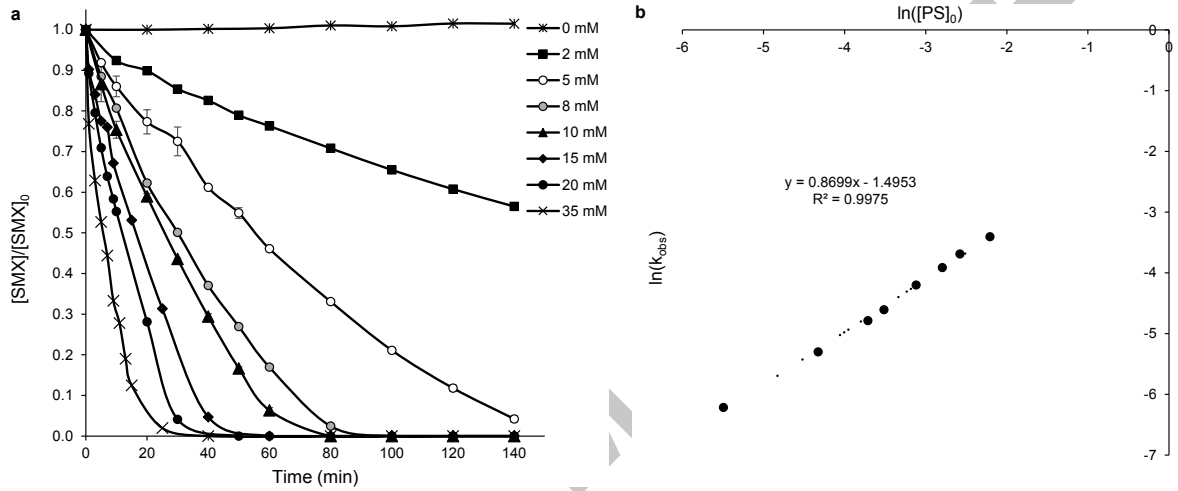

Figure 2: a) SMX degradation for different PS concentrations; b) Determination of relationship between SMX degradation and persulfate dose. Conditions: T=70 °C, $[PS]_0$=0-35 mM, $[SMX]_0$=100 ppm.

3.3 Influence of temperature

The influence of the reaction temperature on heat-activated persulfate oxidation was investigated next. Figure 3a shows the degradation of SMX as a function of time at different temperatures, ranging from 40 °C to 80 °C. It has been shown that PS can be activated at temperatures between 35-130 °C [25]. As shown in Figure 3, the SMX degradation rate is strongly enhanced by increasing the temperature. This is attributed to both an increase in PS activation efficiency, and an increase in observed reaction rate constant: the feasibility of activation of PS was shown to increase with increasing temperature, making the production of radicals easier and next to this, the observed reaction rate is known to increase with the reaction temperature [26]. To determine the temperature dependency of the process, the activation

energy was determined by calculating the pseudo first order reaction rate constant (k_{obs}) of SMX degradation for every temperature T and plotting ln(k_{obs}) as a function of ($1/T$). The activation energy was then defined by the slope of this correlation, and the pre-exponential factor as the intercept on the y-axis, following the Arrhenius equation as expressed in Equations (10) and (11) (Figure 3b).

$$k_{obs} = k_0 * e^{\frac{-E_a}{RT}} \qquad (10)$$

$$\ln(k_{obs}) = \ln(k_0) + \frac{-E_a}{RT} \qquad (11)$$

The activation energy was determined to be 103 kJ/mol. Ji et al. (2015) and Gao et al. (2015) previously reported an activation energy of 119.6 and 130.93 kJ/mol, respectively [16,27]. These results are in fair agreement with the value obtained in this study.

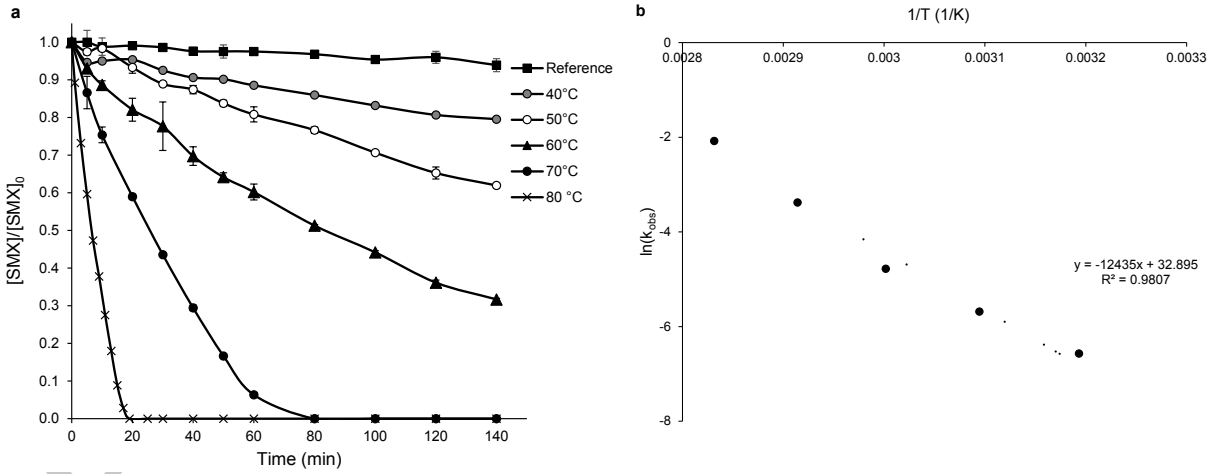

Figure 3: a) SMX degradation for different temperatures; b) Determination of activation energy. Conditions: T=40-80 °C (Reference= room temperature, ± 23 °C), $[PS]_0$=10 mM, $[SMX]_0$=100 ppm.

3.4 Influence of initial SMX concentration

The influence of the initial SMX concentration is shown in Figure 4. The observed reaction rate constant increased with decreasing initial SMX concentration. This is attributed to the ratio between the number of produced radicals and the amount of SMX. In each experiment, it is assumed that the same number of radicals are formed, but as the amount of SMX decreases,

more radicals will be available per unit of SMX which causes the higher observed SMX degradation and higher observed reaction rate constant [28].

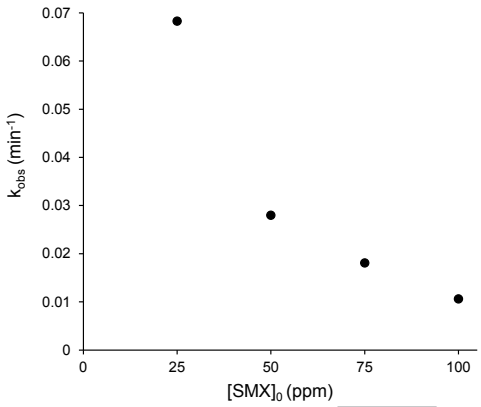

Figure 4: Effect of initial SMX concentration on the observed reaction rate constant. Conditions: T=70 °C, $[PS]_0$=5 mM, $[SMX]_0$=25-100 ppm

3.5 Influence of initial pH

To assess the influence of pH on the heat-activated persulfate oxidation process, the initial pH of the SMX mixture was adjusted to 2.9, 4.6 (not adjusted, indicated as NA), 6.8, 8.7 and 9.

It is important to note that no pH buffer was added, meaning that the pH could change during the reaction. Therefore, the pH was monitored during every experiment. It was observed that the pH decreased from the initial pH to a value close to 3.5 in all experiments (except for the experiments with a pH of 2.9, here the pH remained constant during the observed time). This evolution can only be explained via the produced degradation products. For example, Moradi and Moussavi (2018) suggested that the pH is influenced by carboxylic acids such as formic and acetic acid, which are formed during the degradation of SMX [29].

The degradation of SMX for different initial pH values is shown in Figure 5a. A clear difference in SMX degradation is observed during the first 60-80 min of degradation, after which no further difference between the curves is observed. The latter is attributed to the pH change

during the degradation process: after a reaction time of 60 min, the pH value of the reaction mixture has converged to a value of 3.5 for all experiments, hence no significant difference is further noticed between the experiments.

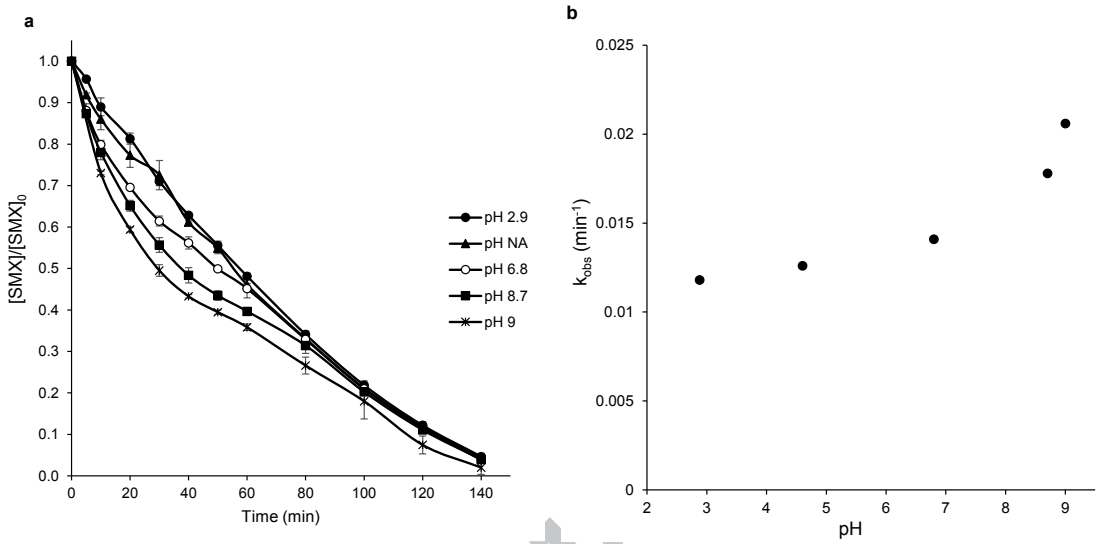

Figure 5: a) SMX degradation for different initial pH; b) Change of k_{obs} as a function of initial pH. Conditions: T= 70 °C, $[PS]_0$=5 mM, $[SMX]_0$=100 ppm.

The difference in SMX degradation during the first 60 min due to a difference in pH is attributed to two causes: (*i*) a change in SMX distribution and (*ii*) the formation of other radicals differing in reactivity. Both causes are dependent on the pH of the reaction mixture. In the studied pH range, SMX exists in different ionization forms (SMX has two pKa values: pKa_1=1.97 and pKa_2=6.16). The occurrence of the different ionization forms of SMX as a function of the pH is depicted in Figure 6. The deprotonated form of SMX is dominant at pH above the pKa_2 of the molecule. Depending on the radicals present, this influences the degradation pathway. Previously, the deprotonated form of SMX was found to be more susceptible for $\bullet SO_4^-$ oxidation [30].

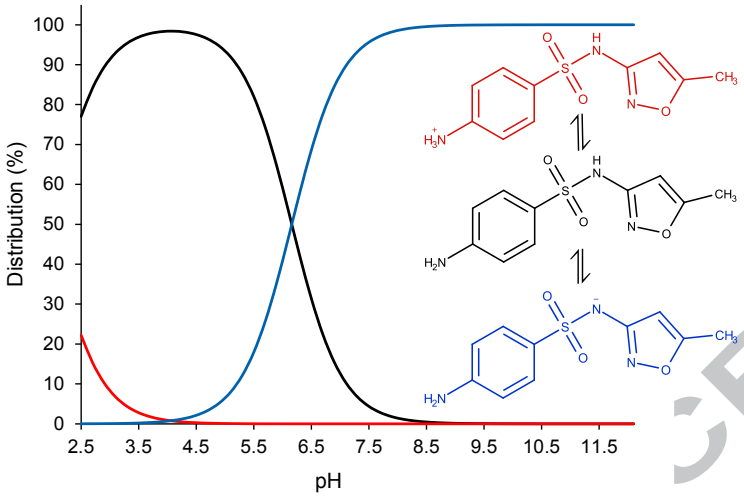

Figure 6: Distribution of SMX as a function of pH. Made in MarvinSketch 18.4 (ChemAxon).

The formation of radicals is also pH dependent. $\bullet SO_4^-$ can react with OH^- ions to form •OH (Equation (12)). Another way to form •OH from $\bullet SO_4^-$, is via the hydrolysis of $\bullet SO_4^-$ (Equation (13)). However, the reaction rate of this reaction is relatively low ($<1\times10^3$ $M^{-1}s^{-1}$, compared to 6.5×10^7 $M^{-1}s^{-1}$ for Equation (12)) [6].

$$\cdot SO_4^- + OH^- \rightarrow SO_4^{2-} + \cdot OH \qquad (12)$$

$$\cdot SO_4^- + H_2O \rightarrow SO_4^{2-} + \cdot OH + H^+ \qquad (13)$$

These produced radicals can also react with SMX. Figure 5b shows the obtained observed reaction rate constant (k_{obs}) as a function of the initial pH. It was determined for the degradation process, considering the first 60 min of reaction only. This figure shows an increase in the observed reaction rate constant with increasing initial pH. This was also observed by Ji et al. [16]. However, they could not identify which of the two causes was responsible for this difference. Since an increase in initial pH causes an increase in the deprotonated form of SMX as well as an increase in •OH formation, both mechanisms can cause the increasing SMX degradation rate. Therefore, in the next section, the radical contributions in the system (at different initial pH values) were investigated.

3.6 Radical contributions

Two techniques were used to investigate which type of radicals play a key role in the heat-activated persulfate oxidation: (*i*) an indirect method using radical scavengers and (*ii*) a direct method using ESR measurements. For the radical scavenging experiments, ethanol (EtOH) was used as a scavenger for both $\bullet SO_4^-$ and •OH, because of its high reaction rate with both types of radical (reaction rate constants of $1.6\text{-}7.7\times10^7$ $M^{-1}s^{-1}$ and $1.2\text{-}2.8\times10^9$ $M^{-1}s^{-1}$ for $\bullet SO_4^-$ and •OH, respectively). Tertiary butanol (TBA) on the other hand, was used as an •OH scavenger, because of its high reaction rate with •OH (reaction rate constant of $3.8\text{-}7.6\times10^8$ $M^{-1}s^{-1}$) and, contrary to EtOH, a lower reaction rate with $\bullet SO_4^-$ (reaction rate constant of $4.0\text{-}9.1\times10^5$ $M^{-1}s^{-1}$) [23]. By adding both scavengers separately and in excess with respect to SMX, the radicals responsible for the degradation were (indirectly) identified. Figure 7 shows the result of the radical scavenging experiments. It is clear that at a pH of 4.6 (NA), the addition of TBA does not result in a decrease in SMX degradation, indicating that, in this process, the degradation of SMX occurs via $\bullet SO_4^-$. This has previously been confirmed by Zhang et al. (2015) who found that, at pH < 7, $\bullet SO_4^-$ was the dominant radical [7]. As previously discussed, •OH is formed at higher pH (Equation (12)). Liang and Su (2009) found that at a pH around 9, both $\bullet SO_4^-$ and •OH are present [31]. Therefore, at an initial pH of 9, a limited difference in SMX degradation between the addition of TBA and the reference experiment is expected. The result hereof is shown in Figure 7b. In this figure, a limited (but significant, as confirmed by a paired t-test (p-value=0.00023)) difference is observed in SMX degradation with and without TBA. The fact that only a limited difference is observed, is probably due to the rapid decrease in pH during all experiments as previously described (the decrease in pH during these experiments was identical with and without scavengers). It also indicates that $\bullet SO_4^-$ is the dominant radical in the degradation process. The previous analysis leads to the conclusion that the increasing

degradation rate at increasing initial pH is attributed to the increased presence of the deprotonated form of SMX in the reaction mixture.

Figure 7 shows that a limited SMX degradation is still observed when adding EtOH to the process, which is probably due to the need for a higher excess ratio of SMX:scavenger. However, due to the relatively low solubility of SMX, this ratio was kept at 1:100 to prevent precipitation.

To further confirm the large contribution of $\bullet SO_4^-$ in this process, a more direct technique, i.e., X-band ESR spectroscopy, was used. For the application of this technique, the formed radicals are initially reacted with a spin trapping agent, forming a stable radical adduct (relative to the radical itself). Each radical adduct has a specific ESR spectrum, enabling the identification and analysis of the different radicals [6]. In this case, the ESR experiments were conducted in DMSO using the spin trapping agent DMPO (see experimental section). Heat activation of persulfate in the presence of the spin trapping agent resulted in a six-line spectrum (Figure S1). This spectrum is in accordance to the spectrum found by Zalibera et al. (2009), who confirmed it as the DMPO-SO_4 spectrum [21]. The figure also shows no presence of the DMPO-OH spectrum, verifying the dominance of $\bullet SO_4^-$ in the reaction mixture and confirming the absence of •OH in this process (at non-adjusted pH). This way, the results of the scavenging experiments are confirmed.

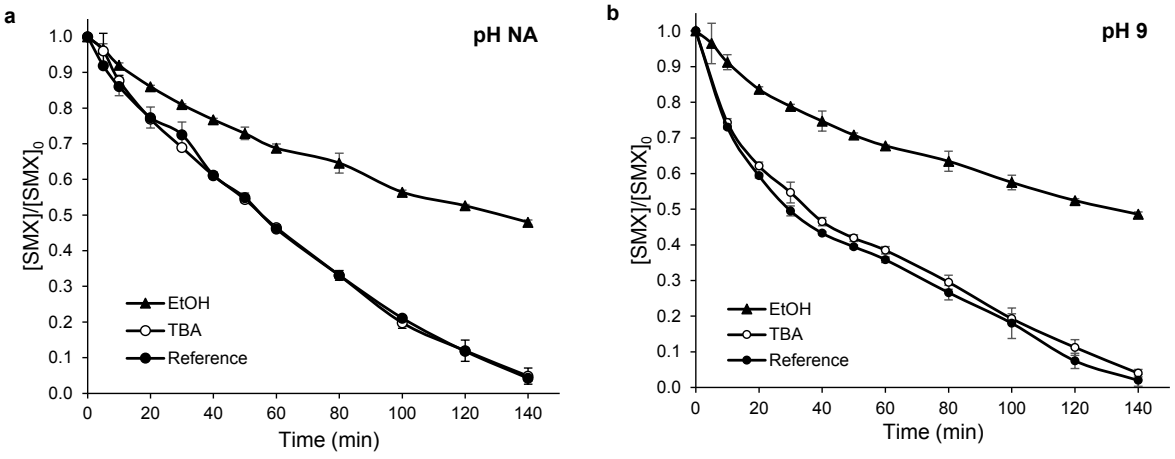

Figure 7: Radical contributions in heat-activated persulfate oxidation. Conditions: T=70 °C, $[PS]_0$= 5 mM, $[SMX]_0$= 100 ppm, molar ratio SMX:scavenger= 1:100, initial pH: a) non-adjusted (NA): 4.6; b) 9.

3.7 Identification of degradation products

3.7.1 Degradation mechanism

Several degradation products were identified with UHPLC-UV-MS. To identify the main routes of degradation, these degradation products were monitored for 140 min during the SMX degradation, using different initial PS concentrations (5, 10 and 35 mM). As previously described, increasing the PS concentration results in an acceleration of the degradation process. This way, the sequence of formation of these products was identified. The structures of the found degradation products are shown in Figure S2. A product with m/z 270 [M-H^+] was identified. The fragmentation pattern of this compound confirmed this degradation product to be hydroxylated-SMX (OH-SMX, observed MS^2 fragments: m/z 204, 172, 124, 108 and 99). The component with m/z 284 [M-H^+], was identified as nitro-SMX (NO_2-SMX, observed MS^2 fragments: m/z 220, 193, 189, 173, 143 and 122). Next to this, m/z 99 [M-H^+] was identified as 3-amino 5-methylisoxazole (observed MS^2 fragments: m/z 72, 71 and 55). These three products were confirmed by comparing their fragments with those found by Gómez-Ramos et al. (2009) [32]. The identity of the product with m/z 99 was additionally verified with an analytical standard, by comparing retention times and observed fragments. Aside from these degradation products, a product with m/z 282 was found. To the best of our knowledge, this transformation product was not yet detected in heat-activated persulfate oxidation. However, it has been detected by Gmurek et al. (2015) during the phototransformation of SMX and was identified as formyl-SMX [33]. Achermann et al. (2017) also found this degradation product in the biotransformation of SMX [34]. It should be noted that the identity of m/z 282 was only confirmed by one fragment (MS^3 fragment: m/z 136 in accordance with Achermann et al. (2017)), therefore its structure should be considered as tentative only.

The degradation of SMX for initial PS concentrations of 5-35 mM was already shown in Figure 2a. The evolution of the degradation products as a function of time for different initial PS concentrations is displayed in Figure S3. This figure shows that a higher initial PS concentration leads to an acceleration of the degradation process. This can be deduced from the observed maximum concentration for each degradation product: at higher PS concentrations, the maximum relative peak area is observed earlier in time. Figure 8 shows the time needed for every degradation product to reach its maximum relative peak area. In this figure, the shortest time needed to reach its maximum relative peak area is observed for m/z 270, indicating that this is the first degradation product formed. For m/z 282 and 284, the time needed is identical at 10 and 35 mM, whereas at 5 mM a difference in time is observed. This indicates that these products are formed simultaneously in the degradation process. However, the formation of m/z 284 is faster. From the degradation mechanism proposed by Ji et al. (2015) and Yang et al. (2017), m/z 284 is formed through a few intermediates, including N4-OH-SMX and NO-SMX before forming NO_2-SMX [16,35]. This is in contrast to m/z 270, which explains the faster formation of m/z 270. For m/z 282, no formation process has been proposed so far.

Finally, m/z 99 needs the longest time to reach its maximum concentration, indicating a slow formation of this product. From the predicted reaction pathways reported by Ji et al. (2015) and Yang et al. (2017), m/z 99 is a product mainly formed through bond cleavage of SMX or substituted byproducts [16,35]. The slow formation is, therefore, probably due to the degradation of SMX and its degradation products, such as m/z 270, 282 and 284, that are only formed later in the degradation process.

Besides the found degradation products in the reaction mixture, a precipitate was formed during the process. This precipitate was collected through filtration and further characterized by dissolution in MeOH and analysis with MS through infusion. The precipitate was found to consist of two products: one with m/z 503 [M-H^+] and one with m/z 519 [M-H^+]. These products

were previously reported by Yang et al. (2017) and are dimeric compounds, formed by coupling of the produced N-centered radicals during degradation [35]. The coupling of two radicals results into a product with m/z 503, and hydroxylation of this compound further leads to a product with m/z 519. The found products were further identified by comparing the fragment ions with those found by Yang et al. (2017) (confirmed MS^2 fragment ions for m/z 503: m/z 439 and 412, for m/z 519: m/z 421) [35].

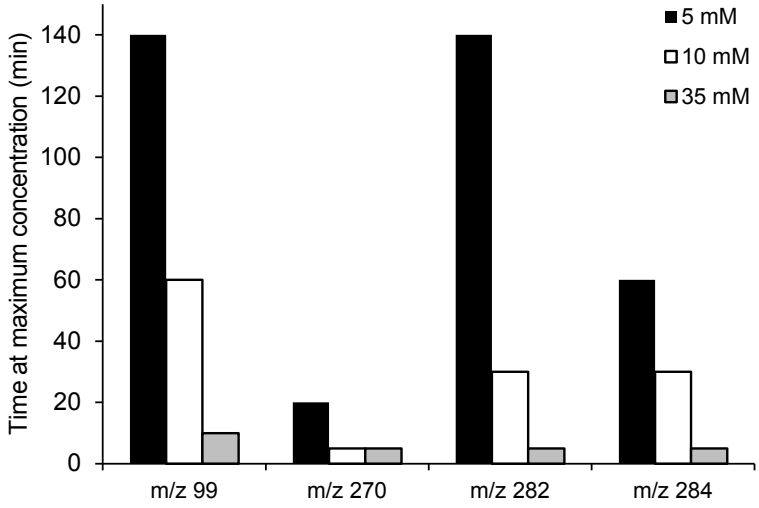

Figure 8: Visualization of the time needed to reach the degradation products' maximal concentration/relative peak area.

3.7.2 Influence of pH on the degradation process

Two types of experiments were carried out to identify the difference in SMX degradation path at different initial pH values: (*i*) identification of the degradation products at an initial pH value of 9 with the addition of TBA to determine the contribution of •OH in the process and (*ii*) identification of the degradation products at initial pH values of 2.9, 4.6, 6.8 and 9 to identify the difference in degradation path due to a difference in SMX distribution. All results are presented as follows: m/z 99 was quantified with an analytical standard and the other degradation products were quantified based on relative peak area. This relative peak area is defined as the peak area of the degradation product at a certain time point, divided by the maximum peak area (observed over the two experiments: reference and TBA). Figure 9 shows the results of the experiments to identify the contribution of •OH. Little to no difference in concentration/relative peak area is observed for most of the degradation products. For m/z 284 however, a difference in its formation is seen. More of this product is formed when the •OH radicals are scavenged, in comparison to the reference degradation, where both •OH and $•SO_4^-$ are present. Thus, the degradation path via formation of m/z 284 is favored by the presence of only $•SO_4^-$. When •OH is present together with $•SO_4^-$, other degradation products with high affinity for $•SO_4^-$ are formed, so that the formation of m/z 284 is inhibited.

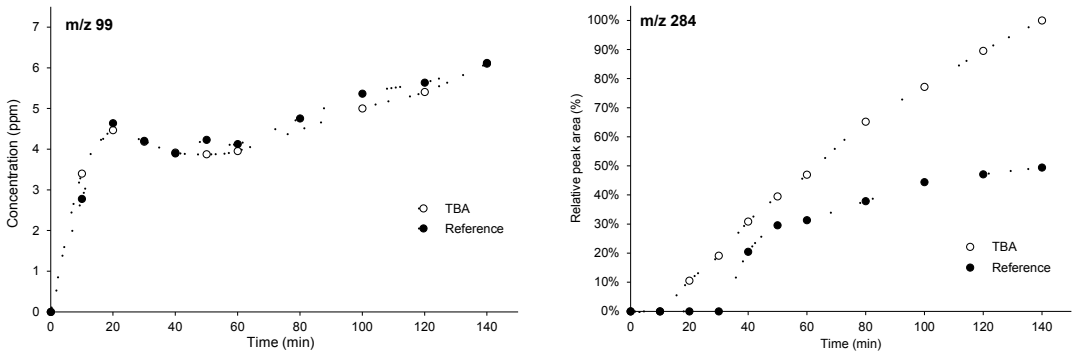

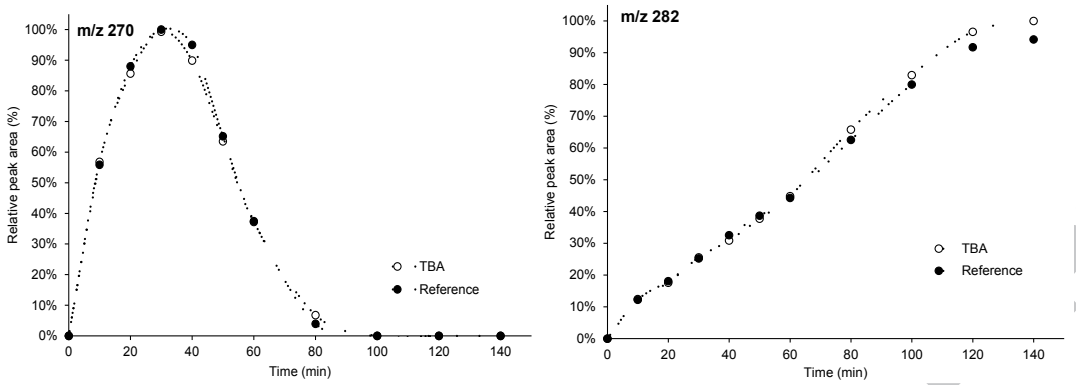

Figure 9: Evolution of degradation products m/z 99, m/z 284, m/z 270 and m/z 282. Conditions: T= 70 °C, $[PS]_0$=5 mM, $[SMX]_0$=100 ppm, initial pH=9, SMX:TBA molar ratio= 1: 100, Reference= no addition of TBA.

Figure 10 shows the results of the investigation of the influence of the SMX distribution on the degradation process. Here, more differences are observed compared to Figure 9, indicating the key role of the SMX distribution on its degradation once more. Degradation product m/z 284 is formed earlier with decreasing initial pH value: at an initial pH value of 9, m/z 284 is formed after 30 min radiation time, whereas at an initial pH value of 6.8, 4.6 and 2.9 m/z 284 is formed after 20 and both 10 min, respectively. After its formation, a clear difference in the curves of m/z 284 is observed for an initial pH of 2.9. This is explained by the hypothesis previously put forward related to the influence of •OH on the formation of this degradation product. At an initial pH of 2.9, $\bullet SO_4^-$ is solely present and the degradation path for formation of m/z 284 is favored.

Degradation product m/z 99 is formed earlier with increasing initial pH value (as is similar to the SMX degradation). This is displayed at the initiation of the reaction: at an initial pH value of 2.9, m/z 99 is only formed after 40 min, for an initial pH value of 4.6 this decreases to 30 min and for initial pH values of 6.8 and 9 this is both after the first sampling point of 10 min. After m/z 99 is formed, all curves follow a more similar trend.

Next to this, there is a clear difference in the formation of m/z 270. Its formation is increased at higher initial pH values. The formation of m/z 270 is thus more likely when the deprotonated form of SMX is present. For m/z 282, a small difference in the curves is observed. The formation increases slightly with increasing initial pH value. Because the formation path of this product is not yet confirmed, the influence of SMX distribution on its formation is unknown.

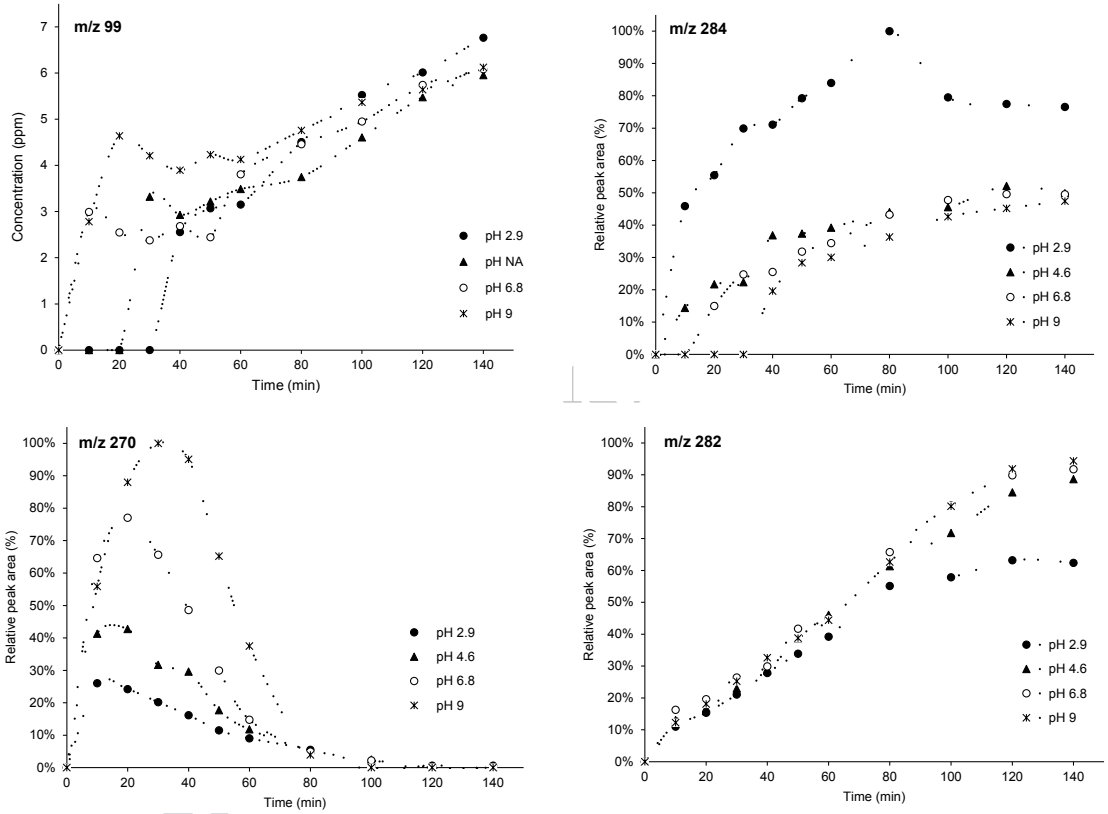

Figure 10: Evolution of degradation products m/z 99, m/z 284, m/z 270 and m/z 282 for different initial pH values. Conditions: T= 70 °C, $[PS]_0$=5 mM, $[SMX]_0$=100 ppm.

3.8 Toxicity assessment

In accordance to Yang et al. (2017), the ECOSAR class chosen for the prediction of the toxicity represents the most toxic estimated values and is depicted in Table 1 [35]. It is important to note that the information provided in the next section involves the toxicity of the individual intermediates. Hence, no information is provided on the toxicity of the reaction mixture.

The acute (LC_{50} for fish (96 hr) and daphnid (48 hr), EC_{50} for green algae (96hr)) and chronic toxicity (ChV, measured for fish, daphnid and green algae) of quantitatively determined products m/z 254 (SMX) and m/z 99 are shown in Figure 11 and 12 respectively. These figures also show the quantitatively determined concentration of the degradation product during the process for initial PS concentrations of 5, 10 and 35 mM. In Figure 11 and 12, the LC_{50} for fish is not shown, because of its relatively high toxicity value ($LC_{50,\ 96\ hr}$= 410.762 ppm and 443.4 ppm for m/z 254 and m/z 99 respectively) relative to the found concentrations in the samples and the toxicity values for daphnid and green algae.

Figure 11a shows the estimated lethal and effect concentrations for SMX, along with the observed SMX degradation as a function of time. For an initial PS concentration of 35 mM, concentrations below both $LC_{50,\ 48hr,\ daphnid}$ and $EC_{50,\ 96hr,\ green\ algae}$ are achieved after a treatment time of approximately 20 min. For an initial PS concentration of 10 mM, this treatment time is extended to 80 min, and for 5 mM the maximum treatment time was insufficient to achieve this. For the chronic values in Figure 11b, the same trend is followed. However, SMX concentrations exceed the $ChV_{daphnid}$ value for initial PS concentrations of 5 and 10 mM. This value is only reached after 120 min treatment time at a concentration of 35 mM.

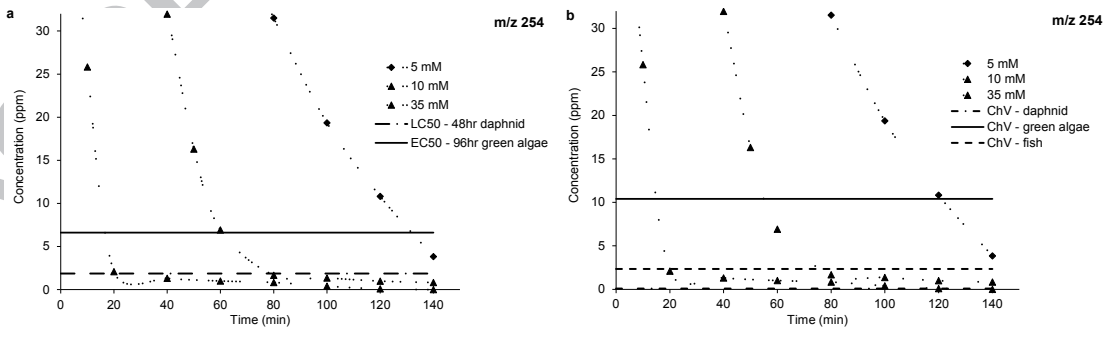

Figure 11: Estimated toxicity of SMX during the SMX degradation process: a) acute toxicity; b) chronic toxicity.

Figure 12 shows the estimated toxicity values for the degradation product with m/z 99. Even for an initial PS concentration of 35 mM, a minimum treatment time of 40 min is necessary to achieve a residual concentration lower than the estimated $LC_{50,\ daphnid}$ and the $EC_{50,\ green\ algae}$

value. For an initial PS concentration of 5 mM, the observed treatment time was insufficient to reach this level of toxicity. As for the chronic values in Figure 12b, the estimated $ChV_{green\ algae}$ value is not reached for an initial PS concentration of 5 mM. A minimal treatment time at a PS concentration of 35 mM of 40 min is required for meeting the $ChV_{daphnid}$ and ChV_{fish} value.

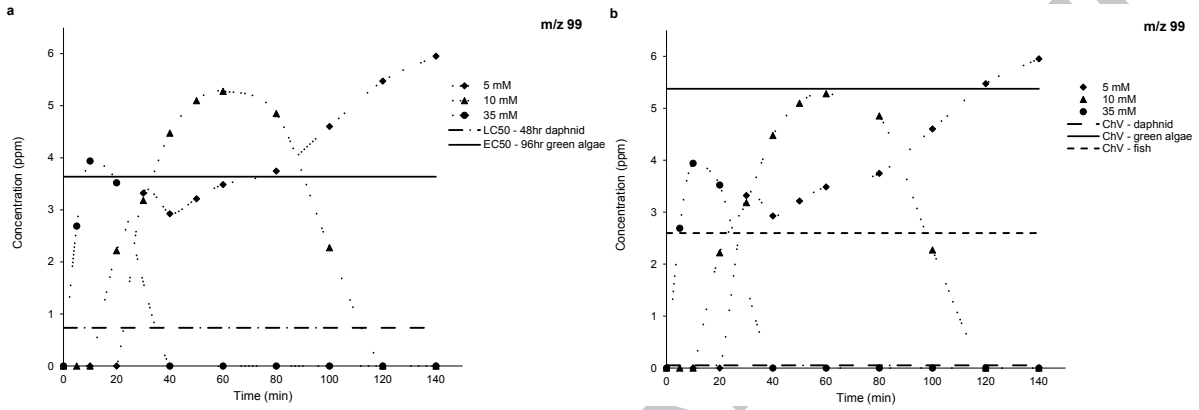

Figure 12: Estimated toxicity of m/z 99 during the SMX degradation process: a) acute toxicity; b) chronic toxicity.

Based on the quantitatively determined degradation products, the residual toxicity of the sample is reduced significantly after a treatment time of 40 min, using an initial PS concentration of 35 mM. Of course, herein, the other degradation products (which could not be quantified) are not included and the very low $ChV_{daphnid}$ value for compound SMX should be underlined. Table 1 provides an overview of the estimated toxicity values for all the found degradation products. Values marked with a grey background indicate an increase in estimated toxicity value relative to SMX. For m/z 503 and 519, the predicted values indicated by * represent values that exceed the solubility limit.

Compared to SMX (m/z 254), m/z 284 and m/z 99 are (generally seen) more toxic. These compounds are thus of specific interest for monitoring the toxicity during the degradation process. For degradation products m/z 503 and 519, also specific care should be taken. Since some toxicity values are below the already low solubility limit, and much lower compared to the toxicity values of SMX, the impact of these products is not to be neglected.

Table 1: Estimated toxicity values for the degradation products by ECOSAR model.

	Fish		Green algae		Daphnid		
Degradation product	$LC_{50,\ 96hr}$ (ppm)	ChV (ppm)	$EC_{50,\ 96hr}$ (ppm)	ChV (ppm)	$LC_{50,\ 48hr}$ (ppm)	ChV (ppm)	ECOSAR Class
m/z 254 (SMX)	410.762	2.337	6.615	10.402	1.872	0.086	Anilines (Unhindered)
m/z 270	943.305	5.485	9.149	13.733	2.012	0.126	Anilines (Unhindered)
m/z 284	306.332	0.33	8.139	5.499	483.427	16.189	Amides
m/z 99	443.424	2.597	3.637	5.375	0.735	0.051	Anilines (Unhindered)
m/z 282	1132.634	104.588	2783.236	936.797	603.632	61.413	Anilines (Hindered)
m/z 503	32.62*	0.097	1.253*	1.74*	23.43*	2.424*	Amides
m/z 519	74.215*	0.166	2.57	2.915	66.507*	5.011	Amides

*not soluble in water, solubility of m/z 503: 0.8073 ppm, solubility of m/z 519: 6.227 ppm

4. Conclusion

The heat-activated persulfate oxidation process for the degradation of SMX was investigated. It was found that this process followed pseudo first order kinetics and a relationship between PS concentration and reaction rate constant was established. The temperature dependence of this process was examined, from where an activation energy of 103 kJ/mol was obtained. The reaction rate constant was found to increase with decreasing initial SMX concentration. Next to this, a difference in SMX degradation was observed at different initial pH values, especially at higher pH values. This was found to be the result of two causes: (*i*) SMX distribution: at higher pH the deprotonated form of SMX was present and (of smaller contribution) (*ii*) formation of •OH at higher pH values. The dominance of $•SO_4^-$ in this process was confirmed by ESR experiments. The degradation of SMX in its degradation products was also investigated and resulted in the identification of six reaction intermediates: m/z 270, 284, 99, 282, 503 and 519. By analyzing these intermediates, the course of the reaction was analyzed and identified in following order: m/z 270 – m/z 284 – m/z 282 – m/z 99. Two reaction products with m/z 503 and 519 were found as precipitates at the end of the reaction process. To distinguish the difference in SMX degradation at different pH values, the influence of •OH distribution on the

degradation path at an initial pH value of 9 was also investigated. Next to this, the degradation path at different initial pH values was determined to evaluate the influence of the SMX distribution (apart from •OH contribution) in the degradation process. The influence of •OH was in the formation of degradation product m/z 284: it was found that this product formation was favored when solely $•SO_4^-$ was present. The influence of the SMX distribution was most explicit in the formation of m/z 270, which was favored at higher initial pH value when the deprotonated value of SMX was present. A prediction of toxicity was carried out using the ECOSAR program for predicting both acute and chronic toxicity of the formed products. From this prediction, a significant reduction of toxicity was observed at a PS concentration of 35 mM and a reaction time of 40 min. However, care should be taken when interpreting these results, as the toxicity values do not consider the influence of mixtures of the degradation products.

Acknowledgements

Hannah Milh holds a PhD fellowship of the Research Foundation – Flanders (FWO) (11D7418N). Agilent Technologies is kindly thanked for providing the Agilent Infinity UHPLC system through a University Relations Grant (3114).

References

[1] C. Gadipelly, A. Pérez-González, G.D. Yadav, I. Ortiz, R. Ibáñez, V.K. Rathod, K. V Marathe, Pharmaceutical Industry Wastewater: Review of the Technologies for Water Treatment and Reuse, Ind. Eng. Chem. Res. 53 (2014) 11571–11592. doi:10.1021/ie501210j.

[2] K.E. Arnold, A.R. Brown, G.T. Ankley, J.P. Sumpter, Medicating the environment: assessing risks of pharmaceuticals to wildlife and ecosystems, Philos. Trans. R. Soc. B Biol. Sci. 369 (2014) 20130569–20130569. doi:10.1098/rstb.2013.0569.

[3] F.A. Caliman, M. Gavrilescu, Pharmaceuticals, personal care products and endocrine disrupting agents in the environment - A review, Clean - Soil, Air, Water. 37 (2009) 277–303. doi:10.1002/clen.200900038.

[4] J. Rivera-Utrilla, M. Sánchez-Polo, M.Á. Ferro-García, G. Prados-Joya, R. Ocampo-Pérez, Pharmaceuticals as emerging contaminants and their removal from water. A review, Chemosphere. 93 (2013) 1268–1287. doi:10.1016/j.chemosphere.2013.07.059.

[5] R. Dewil, D. Mantzavinos, I. Poulios, M.A. Rodrigo, New perspectives for Advanced Oxidation Processes, J. Environ. Manage. 195 (2017) 93–99. doi:10.1016/j.jenvman.2017.04.010.

[6] W.-D. Oh, Z. Dong, T.-T. Lim, Generation of sulfate radical through heterogeneous catalysis for organic contaminants removal: Current development, challenges and prospects, Appl. Catal. B Environ. 194 (2016) 169–201. doi:10.1016/j.apcatb.2016.04.003.

[7] B.T. Zhang, Y. Zhang, Y. Teng, M. Fan, Sulfate radical and its application in decontamination technologies, Crit. Rev. Environ. Sci. Technol. 45 (2015) 1756–1800. doi:10.1080/10643389.2014.970681.

[8] G.P. Anipsitakis, D.D. Dionysiou, Radical generation by the interaction of transition metals with common oxidants, Environ. Sci. Technol. 38 (2004) 3705–3712. doi:10.1021/es035121o.

[9] G.P. Anipsitakis, D.D. Dionysiou, Transition metal/UV-based advanced oxidation technologies for water decontamination, Appl. Catal. B Environ. 54 (2004) 155–163. doi:10.1016/j.apcatb.2004.05.025.

[10] L.W. Matzek, K.E. Carter, Activated persulfate for organic chemical degradation: A

review, Chemosphere. 151 (2016) 178–188. doi:10.1016/j.chemosphere.2016.02.055.

[11] Y. Liu, S. Wang, Y. Wu, H. Chen, Y. Shi, M. Liu, W. Dong, Degradation of ibuprofen by thermally activated persulfate in soil systems, Chem. Eng. J. 356 (2019) 799–810. doi:10.1016/j.cej.2018.09.002.

[12] J. Cai, M. Zhou, W. Yang, Y. Pan, X. Lu, K.G. Serrano, Degradation and mechanism of 2,4-dichlorophenoxyacetic acid (2,4-D) by thermally activated persulfate oxidation, Chemosphere. 212 (2018) 784–793. doi:10.1016/j.chemosphere.2018.08.127.

[13] Y. Aimer, O. Benali, K. Groenen Serrano, Study of the degradation of an organophosphorus pesticide using electrogenerated hydroxyl radicals or heat-activated persulfate, Sep. Purif. Technol. 208 (2019) 27–33. doi:10.1016/j.seppur.2018.05.066.

[14] S. Norzaee, M. Taghavi, B. Djahed, F. Kord Mostafapour, Degradation of Penicillin G by heat activated persulfate in aqueous solution, J. Environ. Manage. 215 (2018) 316–323. doi:10.1016/j.jenvman.2018.03.038.

[15] I.A. Ike, K.G. Linden, J.D. Orbell, M. Duke, Critical review of the science and sustainability of persulphate advanced oxidation processes, Chem. Eng. J. 338 (2018) 651–669. doi:10.1016/j.cej.2018.01.034.

[16] Y. Ji, Y. Fan, K. Liu, D. Kong, J. Lu, Thermo activated persulfate oxidation of antibiotic sulfamethoxazole and structurally related compounds, Water Res. 87 (2015) 1–9. doi:10.1016/j.watres.2015.09.005.

[17] C. Liang, C.F. Huang, N. Mohanty, R.M. Kurakalva, A rapid spectrophotometric determination of persulfate anion in ISCO, Chemosphere. 73 (2008) 1540–1543. doi:10.1016/j.chemosphere.2008.08.043.

[18] G. Desmet, D. Cabooter, Are Short Columns Always The Best Option ?, LC-GC Eur. 22

(2009) 70–77. http://www.chromatographyonline.com/are-short-columns-always-best-option (accessed February 7, 2019).

[19] M. Favier, A. Van Schepdael, D. Cabooter, High-Resolution MS and MS n Investigation of UV Oxidation Products of Phenazone-type Pharmaceuticals and Metabolites, Chromatographia. (2018). doi:10.1007/s10337-018-3668-0.

[20] M. Favier, R. Dewil, K. Van Eyck, A. Van Schepdael, D. Cabooter, High-resolution MS and MSn investigation of ozone oxidation products from phenazone-type pharmaceuticals and metabolites, Chemosphere. 136 (2015) 32–41. doi:10.1016/j.chemosphere.2015.04.010.

[21] M. Zalibera, P. Rapta, A. Staško, L. Brindzová, V. Brezová, Thermal generation of stable $SO_4^{\cdot-}$-spin trap adducts with super-hyperfine structure in their EPR spectra: An alternative EPR spin trapping assay for radical scavenging capacity determination in dimethylsulphoxide, Free Radic. Res. 43 (2009) 457–469. doi:10.1080/10715760902846140.

[22] J. Ma, H. Li, L. Chi, H. Chen, C. Chen, Changes in activation energy and kinetics of heat-activated persulfate oxidation of phenol in response to changes in pH and temperature, Chemosphere. 189 (2017) 86–93. doi:10.1016/j.chemosphere.2017.09.051.

[23] Y. Chen, P. Deng, P. Xie, R. Shang, Z. Wang, S. Wang, Heat-activated persulfate oxidation of methyl- and ethyl-parabens: Effect, kinetics, and mechanism, Chemosphere. 168 (2017) 1628–1636. doi:10.1016/j.chemosphere.2016.11.143.

[24] R.L. Johnson, P.G. Tratnyek, R.O.B. Johnson, Persulfate persistence under thermal activation conditions, Environ. Sci. Technol. 42 (2008) 9350–9356. doi:10.1021/es8019462.

[25] A. Tsitonaki, B. Petri, M. Crimi, H. Mosbaek, R.L. Siegrist, P.L. Bjerg, In Situ Chemical Oxidation of Contaminated Soil and Groundwater Using Persulfate: A Review, Crit. Rev. Environ. Sci. Technol. 40 (2010) 55–91. doi:10.1080/10643380802039303.

[26] Y. Ji, C. Dong, D. Kong, J. Lu, Q. Zhou, Heat-activated persulfate oxidation of atrazine: Implications for remediation of groundwater contaminated by herbicides, Chem. Eng. J. 263 (2015) 45–54. doi:10.1016/j.cej.2014.10.097.

[27] Y.Q. Gao, N.Y. Gao, Y. Deng, D.Q. Yin, Y. Sen Zhang, W.L. Rong, S.D. Zhou, Heat-activated persulfate oxidation of sulfamethoxazole in water, Desalin. Water Treat. 56 (2015) 2225–2233. doi:10.1080/19443994.2014.960471.

[28] L. Bu, Z. Shi, S. Zhou, Modeling of Fe(II)-activated persulfate oxidation using atrazine as a target contaminant, Sep. Purif. Technol. 169 (2016) 59–65. doi:10.1016/j.seppur.2016.05.037.

[29] M. Moradi, G. Moussavi, Investigation of chemical-less UVC/VUV process for advanced oxidation of sulfamethoxazole in aqueous solutions: Evaluation of operational variables and degradation mechanism, Sep. Purif. Technol. 190 (2018) 90–99. doi:10.1016/j.seppur.2017.08.006.

[30] C. Tan, N. Gao, Y. Deng, N. An, J. Deng, Heat-activated persulfate oxidation of diuron in water, Chem. Eng. J. 203 (2012) 294–300. doi:10.12030/j.cjee.201501113.

[31] C. Liang, H.W. Su, Identification of sulfate and hydroxyl radicals in thermally activated persulfate, Ind. Eng. Chem. Res. 48 (2009) 5558–5562. doi:10.1021/ie9002848.

[32] M. del M. Gómez-Ramos, M. Mezcua, A. Agüera, A.R. Fernández-Alba, S. Gonzalo, A. Rodríguez, R. Rosal, Chemical and toxicological evolution of the antibiotic sulfamethoxazole under ozone treatment in water solution, J. Hazard. Mater. 192 (2011)

18–25. doi:10.1016/j.jhazmat.2011.04.072.

[33] M. Gmurek, H. Horn, M. Majewsky, Phototransformation of sulfamethoxazole under simulated sunlight: Transformation products and their antibacterial activity toward Vibrio fischeri, Sci. Total Environ. 538 (2015) 58–63. doi:10.1016/j.scitotenv.2015.08.014.

[34] S. Achermann, V. Bianco, C. Mansfeldt, B. Vogler, B.A. Kolvenbach, P.F. Corvini, K. Fenner, Biotransformation of Sulfonamide Antibiotics in Activated Sludge: Formation of Pterin-Conjugates Leads to Sustained Risk, Environ. Sci. Technol. (2017). doi:10.1021/acs.est.7b06716.

[35] Y. Yang, X. Lu, J. Jiang, J. Ma, G. Liu, Y. Cao, W. Liu, J. Li, S. Pang, X. Kong, C. Luo, Degradation of sulfamethoxazole by UV, UV/H2O2and UV/persulfate (PDS): Formation of oxidation products and effect of bicarbonate, Water Res. 118 (2017) 196–207. doi:10.1016/j.watres.2017.03.054.